

Strengthening security and noise resistance in one-way quantum key distribution protocols through hypercube-based quantum walks

David Polzoni¹, Tommaso Bianchi¹, and Mauro Conti^{1,2}

¹ University of Padova, Padova, Italy
david.polzoni@studenti.unipd.it
tommaso.bianchi@phd.unipd.it
mauro.conti@unipd.it

² Örebro University, Örebro, Sweden

Abstract. Quantum Key Distribution (QKD) is a foundational cryptographic protocol that ensures information-theoretic security. However, classical protocols such as BB84, though favored for their simplicity, offer limited resistance to eavesdropping, and perform poorly under realistic noise conditions. Recent research has explored the use of discrete-time Quantum Walks (QWs) to enhance QKD schemes. In this work, we specifically focus on a one-way QKD protocol, where security depends exclusively on the underlying Quantum Walk (QW) topology, rather than the details of the protocol itself.

Our paper introduces a novel protocol based on QWs over a hypercube topology and demonstrates that, under identical parameters, it provides significantly enhanced security and noise resistance compared to the circular topology (i.e., state-of-the-art), thereby strengthening protection against eavesdropping. Furthermore, we introduce an efficient and extensible simulation framework for one-way QKD protocols based on QWs, supporting both circular and hypercube topologies. Implemented with IBM's software development kit for quantum computing (i.e., Qiskit), our toolkit enables noise-aware analysis under realistic noise models. To support reproducibility and future developments, we release our entire simulation framework as open-source. This contribution establishes a foundation for the design of topology-aware QKD protocols that combine enhanced noise tolerance with topologically driven security.

Keywords: Quantum Key Distribution · Quantum Walks · Hypercubes.

1 Introduction

Quantum Key Distribution (QKD) is a core application of quantum cryptography, allowing two parties to establish a shared secret key with security guaranteed by quantum mechanics, since any eavesdropping attempt that disturbs the system becomes detectable. The first protocols, BB84 [5] and E91 [18], laid the foundation for modern implementations, which now include commercial systems, long-distance links, and even satellite-based communication [57]. Quantum

Walks (QWs), introduced by Aharonov et al. [2], extend classical random walks into the quantum domain and are central to quantum computing. Their cryptographic applications are emerging, such as the protocol of Rohde et al. [44], which enables quantum homomorphic encryption, allowing servers to process encrypted quantum data while preserving privacy.

Contributions. Our work builds on Vlachou et al. [51], who used Quantum Walk (QW) properties to design secure QKD protocols, including a one-way (prepare-and-measure) scheme with a security proof against full man-in-the-middle attacks on circle graphs (i.e., current state-of-the-art). We extend this approach by generalizing the security proof to arbitrary regular topologies and introducing a hypercube-based QWs protocol. We also develop a realistic, replicable Qiskit model for simulating QWs on both circle and hypercube topologies and use it to implement the one-way QKD protocol. Simulations under Qiskit’s built-in noise models show that the hypercube-based protocol outperforms the state-of-the-art in both security and noise resilience. In summary, our contributions are:

- We introduce a novel one-way QKD protocol based on discrete-time QWs over hypercube topologies, offering a new direction beyond the circular structures;
- We develop robust, flexible, and extensible Qiskit-based models to simulate discrete-time QWs on both circular and hypercube topologies, enabling systematic evaluation across graph structures;
- We extend prior findings that the security of QW-based QKD protocols is determined solely by the underlying walk structure, generalizing this dependence to arbitrary topologies, and demonstrate that hypercube-based QWs achieve higher security by providing increased resistance to eavesdropping;
- We implement and compare a one-way QKD protocol over both QWs models, introducing a unified simulation framework for such a comparative study within the Qiskit environment;
- We show that the hypercube-based protocol improves the maximally tolerated Quantum Error Rate (QER) under depolarizing noise by approximately 20%, and by 13% under combined amplitude-phase damping, compared to the circular case, under identical conditions.

We have made the source code publicly available while preserving anonymity. It can be accessed through the following link:

<https://anonymous.4open.science/r/1W-QKD-Quantum-Walks-891E>.

Organization. The rest of the paper is organized as follows: Section 2 reviews related works and state-of-the-art solutions, while Section 3 provides the necessary background knowledge for this work. Section 4 presents the one-way QKD protocol under analysis, including its security proof. In Section 5, we describe the Qiskit-based implementation of QWs and the corresponding QKD protocol. Then, Section 6 analyzes the protocol’s security for both topologies, followed by an evaluation of its noise resilience in Section 7. Finally, Section 8 addresses limitations and possible practical attacks, and Section 9 reports our conclusions.

2 Related works

This section reviews related works defining the state-of-the-art prior to our contribution. The main reference for QKD protocols based on QWs is Vlachou et al. [51], who proposed a secure protocol with verification against full man-in-the-middle attacks. They also present a one-way QKD protocol, supported by a security proof from its entanglement-based version, and explore a semi-quantum variant. The most advanced implementation of the one-way protocol uses a circular topology, analyzing noise resistance under a generalized Pauli channel and providing the maximally tolerated Quantum Error Rate (QER), serving as the state-of-the-art reference. Building on this, we propose a hypercube-based QWs protocol that enhances both security and noise resilience, achieving improved robustness and a higher tolerated QER under the same conditions. For Qiskit-based QWs implementation, we follow Douglas et al. [16], who define discrete-time QW on general undirected graphs. Each vertex v_i with degree d_i is split into d_i subnodes, and the shift operator $S(v_i, a_i) = (v_j, a_j)$ moves states along edges $(v_i, v_j) \in E$, while the coin operator mixes amplitudes among subnodes via a $d_i \times d_i$ unitary matrix. For a circle, two subnodes per node are encoded with $\lceil \log_2(n) \rceil$ qubits plus one subnode qubit; the coin acts on the subnode qubit, and the shift operator performs cyclic permutations via I and D gates:

$$S = (I \otimes |1\rangle + D \otimes |0\rangle).$$

This framework scales efficiently to hypercube-based QWs, which require larger state and coin spaces, enabling our hypercube-based QKD protocol, as detailed in the following sections.

3 Background

In this section, we present the theoretical background relevant to our work. We begin by reviewing the fundamentals of quantum walks and the quantum gates involved. We then describe the formal models that govern quantum walks on both circular and hypercube structures.

3.1 Quantum walks basics and quantum gates

This paper compares circle and hypercube-based QWs. Unlike classical random walks, where the next state depends only on the current one [54], QWs explore all paths simultaneously via quantum superposition [50]. In coined QWs, the walker's position resides in an n -dimensional space with 2^n positions, encoded in $\mathcal{H} = \mathcal{H}_c \otimes \mathcal{H}_p$, where $\mathcal{H}_c = \{|0\rangle, |1\rangle\}$ is the coin space and $\mathcal{H}_p = \{|j\rangle : j = 0, \dots, n-1\}$ the position space. Evolution is governed by coin and shift operators, producing the unitary operator:

$$U = S \cdot (C \otimes I), \tag{1}$$

where S updates positions based on the coin state, C is a coin operator, and I preserves the walker's state. Some classical random walk principles can extend to QWs [35], with the system after t steps given by:

$$|\psi(t)\rangle = U^t |\psi(0)\rangle. \quad (2)$$

To construct our QW models, we employ the Pauli- X (i.e., NOT), Hadamard (H), and phase (S) gates, which serve respectively to initialize the walker's position, create coin superpositions, and balance the evolution through phase shifts [33].

3.2 Circle-based quantum walks

In this context, following the modeling from Vlachou et al. [51], the walker moves between discrete positions on a circle. The Hilbert space \mathcal{H} , describing the QW, is the tensor product $\mathcal{H} = \mathcal{H}_p \otimes \mathcal{H}_c$, where \mathcal{H}_p is spanned by position states $\{|x\rangle : x \in 0, \dots, P-1\}$, with P denoting the number of discrete positions, and \mathcal{H}_c by the coin states $\{|R\rangle, |L\rangle\}$, representing heads and tails. The evolution of the quantum walk for one step is governed by the unitary operator:

$$U = S \cdot (R_c \otimes I), \quad (3)$$

where I is the identity operator in \mathcal{H}_p , and R_c is a rotation in \mathcal{H}_c . In its generic matrix form, R_c can be written as:

$$R_c(\phi, \theta) = \begin{bmatrix} e^{i\phi} \cos(\theta) & e^{i\phi} \sin(\theta) \\ -e^{-i\phi} \sin(\theta) & e^{-i\phi} \cos(\theta) \end{bmatrix}, \quad (4)$$

where ϕ denotes the phase angle of the rotation, and θ represents the actual rotation angle. The shift operator S moves the walker one position to the right or left on the circle based on its coin state. Explicitly, S is defined as:

$$S = \sum_{x=0}^{P-1} (|x+1 \pmod{P}\rangle \langle x| \otimes |R\rangle \langle R| + |x-1 \pmod{P}\rangle \langle x| \otimes |L\rangle \langle L|). \quad (5)$$

Depending on the coin state, this operator shifts the walker either clockwise or counterclockwise. Since the walker is on a circle, position P is identified with position 0, creating a continuous loop of discrete steps.

3.3 Hypercube-based quantum walks

The representation of the hypercube model for QWs can be formulated based on the approach presented by Portugal [34]. In that case, the coin space, denoted as $\mathcal{H}_c = \mathcal{H}^n$, corresponds to the state of the quantum coin, which can be in a superposition of n possible states. The walker space, denoted as $\mathcal{H}_p = \mathcal{H}^{2^n}$, represents the possible positions of the walker, with each position corresponding

to a binary string of length n , leading to 2^n distinct positions. The total state of the system is the tensor product of these two spaces: $\mathcal{H} = \mathcal{H}_c \otimes \mathcal{H}_p$. This combined space can be defined as the set of all possible states:

$$\mathcal{H} = \{|a\rangle \otimes |v\rangle : 0 \leq a < n, v \in \{(00 \dots 00)_2, (00 \dots 01)_2, \dots, (11 \dots 11)_2\}\}, \quad (6)$$

where $|a\rangle$ corresponds to the coin state, and $|v\rangle$ corresponds to the binary representation of the walker's position. The value of a determines the position in the walker space where the next move occurs. Specifically, a identifies which bit in the position vector $|v\rangle$ has to be flipped. When the coin state is $|a\rangle$, the shift operator will flip the a -th bit of the walker's current position $|v\rangle$, thereby determining the walker's next position. Regarding the coin operator, we can apply a generic R_c , as defined in Equation 4, to each coin qubit. However, for the hypercube topology, the optimal choice is theoretically the Grover coin [34], which can be compactly expressed as:

$$G = \frac{2}{n} J_n - I_n, \quad (7)$$

where n is the number of positions in the QW, I_n is the $n \times n$ identity matrix, and J_n is the $n \times n$ all-ones matrix. Now, let's examine the shift operator S , which determines how the walker moves across the hypercube based on the coin state. To formalize this, let e_a represent a vector with a single 1 in the a -th position and 0 everywhere else. The shift operator S is then defined as:

$$S(|a\rangle \otimes |v\rangle) = |a\rangle \otimes |v \oplus e_a\rangle, \quad (8)$$

where the system's state consists of two parts:

- $|a\rangle$: coin state, which determines the bit to modify. It specifies the position a in the binary representation of the walker's position $|v\rangle$;
- $|v\rangle$: walker's current position, represented as a binary string corresponding to a node on the hypercube.

The walker's position is updated by flipping the bit at position a . This is done using the binary XOR operation (\oplus) between the walker's position v and a vector e_a . Consequently, after applying S , the coin state $|a\rangle$ remains unchanged, while the walker's position is updated to reflect the movement imposed by the coin. Moreover, the final unitary operator U governing the walk can be defined using Equation 1, where the coin operator C is chosen as either the generic rotation coin (see Equation 4) or the Grover coin (see Equation 7).

4 One-way QKD using hypercube-based quantum walks

This section presents our one-way QKD protocol using QWs on a P -dimensional hypercube within a prepare-and-measure framework. Building on Vlachou et al. [51], we replace the circle topology with a hypercube, expanding the state

space from 2^P to 2^P basis states. This exponential growth enriches interference patterns, reduces predictability, and enhances resilience to eavesdropping and noise, improving security without requiring entanglement or quantum memory.

4.1 Protocol description

We begin by defining the shared public parameters P , t , ϕ and θ , where:

- P : dimension of the position space of the quantum walk;
- t : number of steps performed in the QW evolution;
- ϕ, θ : coin parameters.

As previously defined in Equation 3, we can express using U the QW operator, where U is publicly known to all parties. Next, we introduce the F operator, which acts on the coin space \mathcal{H}_c before the QW evolution, rather than as a post-processing operator. This adjustment ensures that the coin state is prepared in a specific way before the QW begins, rather than altering the coin state after the walk has been completed. In our case, the operator F can be either the identity (I), the Hadamard gate (denoted as \tilde{X}), or a cascade of a Hadamard gate followed by a phase gate ($Y = H \cdot S$), where \tilde{X} and Y are defined as follows:

$$\tilde{X} = H = \frac{1}{\sqrt{2}} \begin{bmatrix} 1 & 1 \\ 1 & -1 \end{bmatrix}, Y = H \cdot S = \frac{1}{\sqrt{2}} \begin{bmatrix} 1 & 1 \\ i & -i \end{bmatrix}. \quad (9)$$

In general, the operator F is optional, and when no transformation is applied, it is set to $F = I$. For clarity, note that \tilde{X} here refers to the Hadamard gate (H), not the classical X gate, while Y represents a combination of Hadamard and phase gates ($Y = H \cdot S$), used for coin state balancing. This notation, adopted for consistency with Vlachou et al. [51], allows us to explore different transformations on the coin state to fine-tune the QW behavior. Let $|\psi_i\rangle$ represent the protocol's state after the complete evolution, defined as:

$$|\psi_i\rangle = U^t \cdot (I \otimes F) |i\rangle, \text{ for } |i\rangle \in \mathcal{H}_p \otimes \mathcal{H}_c. \quad (10)$$

Moreover, the orthonormal basis $\{|\psi_i\rangle\}$ is referred to as the *QW* basis, derived from the computational basis \mathcal{Z} through the QW evolution. It is important to note that the unitary operator governing this basis change is the same unitary operator that describes the QW process. The protocol consists of N iterations, each comprising the following steps:

1. Alice (A) chooses a random bit $w_A \in \{0, 1\}$ and random $i_A \in \{0, \dots, 2^P - 1\}$. Then, depending on w_A value:
 - If $w_A = 0$, Alice prepares and sends to Bob (B), over the public quantum channel, the 2^P -dimensional state:

$$|\psi_i\rangle = |i_A\rangle. \quad (11)$$

- If $w_A = 1$, Alice prepares and sends to Bob, over the public quantum channel, the 2^P -dimensional state:

$$|\psi_i\rangle = U^t \cdot (I \otimes F) |i_A\rangle. \quad (12)$$

- Bob chooses a random bit $w_B \in \{0, 1\}$. Then, depending on w_B value:
 - If $w_B = 0$, Bob measures the received state in the computational \mathcal{Z} basis;
 - If $w_B = 1$, Bob measures in the \mathcal{QW} basis or, alternatively, he inverts the QW by applying $(U^t)^{-1} = U^{-t}$ and measures the resulting state in the \mathcal{Z} basis.

Let j_B be the outcome in each case.

- Alice and Bob reveal w_A and w_B via a classical authenticated channel. Then, based on their choices:
 - If $w_A = w_B$, i_A and j_B contribute to the raw key;
 - If $w_A \neq w_B$, the iteration is discarded.

After completing the process, Alice and Bob use a cut-and-choose method [55] to detect eavesdropping by selecting a subset of iterations for parameter estimation and removing them from the raw key. This estimates the disturbances Q_z and Q_w in the \mathcal{Z} and \mathcal{QW} bases, which are ideally zero. If disturbances remain below a defined threshold, they proceed with error correction and privacy amplification. Finally, a scheme of the protocol is provided in Appendix A.

4.2 Security proof

In this subsection, we prove the security of the proposed protocol by deriving an equivalent entanglement-based version, following standard QKD techniques [6,27]. Establishing security for the entanglement-based protocol also validates the corresponding prepare-and-measure version [6,14,13] and can extend to device-independent QKD under suitable device assumptions [53]. The proof builds on Vlachou et al. [51] and can be adapted to hypercube-based QKD with minor modifications. For the entanglement-based protocol, each of the N iterations modifies the initial steps as follows:

- Alice (A) prepares the entangled state:

$$|\Psi_0\rangle = \frac{1}{\sqrt{2^P}} \sum_{i=0}^{2^P-1} |i, i\rangle_{AB}. \quad (13)$$

Then, she sends to Bob (B) the second portion of the prepared entangled state ($|\Psi_0\rangle_B$), while retaining the first portion ($|\Psi_0\rangle_A$) in her private lab;

- Alice and Bob independently choose two random bits, $w_A \in \{0, 1\}$ and $w_B \in \{0, 1\}$. If $w_A = 0$, Alice measures $|\Psi_0\rangle_A$ in the computational \mathcal{Z} basis. Otherwise, she measures in the \mathcal{QW} basis. Bob similarly measures $|\Psi_0\rangle_B$ according to w_B . Their measurement outcomes are recorded as i_A for Alice and j_B for Bob.

After these adjustments, the entanglement-based version proceeds as the prepare-and-measure counterpart, following the same basis reconciliation and subsequent steps. Additionally, Appendix A includes a depiction of the entanglement-based scheme. Next, we demonstrate the security of the hypercube entanglement-based protocol by first making three assumptions:

- A_1 : Alice and Bob only use iterations where $w_A = w_B = 0$ for their raw key;
- A_2 : Eve is limited to collective attacks, where she independently attacks each protocol iteration but can perform a joint measurement of her ancilla at any future time;
- A_3 : Eve prepares the states that Alice and Bob hold.

Assumption A_1 simplifies computations and can be discarded later. Alternatively, Alice and Bob can intentionally bias their selection of measurement bases to increase the probability that both choose $w_A = w_B = 0$, following a similar strategy used in the BB84 protocol. Moreover, assumption A_2 can be removed later using a de-Finetti argument, yielding security in the asymptotic limit without degrading the key-rate [43,12,42]. It is worth noting that removing assumption A_2 is sufficient to establish the protocol's security. Instead, assumption A_3 grants more power to Eve: if security is shown with A_3 , it holds even when A_3 is removed. Additionally, it is important to underline that this proof focuses exclusively on the asymptotic regime, where the key-rate expression is unaffected by finite-size effects, a standard assumption in theoretical QKD security proofs [45], while finite-key analyses provide the necessary corrections for practical implementations [47]. Given A_2 and A_3 , Alice, Bob, and Eve, after N iterations, share a quantum state $\hat{\rho}_{ABE}^{\otimes N}$, where:

$$\hat{\rho}_{ABE} \in \mathcal{H}_A \otimes \mathcal{H}_B \otimes \mathcal{H}_E, \text{ with } \mathcal{H}_A \equiv \mathcal{H}_B \equiv \mathcal{H}_p \otimes \mathcal{H}_c.$$

Note that Eve, as an all-powerful adversary, is not limited in the choice of her Hilbert space \mathcal{H}_E . After information reconciliation and privacy amplification, Alice and Bob share a secret key of size $\ell(N)$. Under the assumption of collective attacks (A_2), the Devetak-Winter key-rate expression [15] can be written explicitly as:

$$r = \lim_{N \rightarrow \infty} \frac{\ell(N)}{N} = S(A|E) - H(A|B). \quad (14)$$

Let A_z and A_w be random variables representing Alice's system when measured in the \mathcal{Z} or \mathcal{QW} basis, respectively, with B_z and B_w defined similarly for Bob. Under assumption A_1 , we are interested in:

$$r = S(A_z|E) - H(A_z|B_z). \quad (15)$$

Computing $H(A_z|B_z)$ is straightforward, given the probabilities:

$$p_{i,j}^z = \mathbb{P}(i_A = i, j_B = j \mid w_A = w_B = 0). \quad (16)$$

The challenge lies in bounding the Von-Neumann entropy $S(A_z|E)$. To do this, we apply an uncertainty relation [8] which states that, for any density matrix $\hat{\rho}_{ABE} \in \mathcal{H}_A \otimes \mathcal{H}_B \otimes \mathcal{H}_E$, if Alice and Bob perform measurements with POVMs:

$$\hat{M}_0 = \{\hat{M}_x^{(0)}\}_x \text{ or } \hat{M}_1 = \{\hat{M}_x^{(1)}\}_x,$$

then:

$$S(A_0|E) + H(A_1|B) \geq \log \frac{1}{c}, \quad (17)$$

where c is given by:

$$c = \max_{x,y} \|\hat{M}_x^{(0)} \hat{M}_y^{(1)}\|_\infty^2, \quad (18)$$

considering $\|\cdot\|_\infty$ as the operator norm, with A_i representing a random variable that describes Alice's system after applying the measurement \hat{M}_i . Similarly, we can define B_i for Bob's system. Assuming measurements \hat{M}_0 are used for key distillation, we derive the following Devetak-Winter key-rate:

$$r = S(A_0|E) - H(A_0|B_0) \geq \log \frac{1}{c} - H(A_0|B_0) - H(A_1|B), \quad (19)$$

then, building on the principle that measurements can only increase entropy, we get:

$$r \geq \log \frac{1}{c} - H(A_0|B_0) - H(A_1|B_1). \quad (20)$$

In our scenario, we set the measurement operators as:

$$\hat{M}_x^{(0)} = |x\rangle\langle x| \text{ for } \mathcal{Z} \text{ basis, } \hat{M}_x^{(1)} = |\psi_x\rangle\langle\psi_x| \text{ for } \mathcal{QW} \text{ basis,}$$

where, in the context of hypercube-based quantum walks, we consider $x \in \{0, 1, \dots, 2^P - 1\}$, and let $|\psi_x\rangle$ be defined as $|\psi_x\rangle = \sum_i \alpha_{x,i} |i\rangle$. Then, it follows directly that:

$$\|\hat{M}_x^{(0)} \hat{M}_y^{(1)}\|_\infty^2 = |\alpha_{x,y}|^2, \text{ for all } x, y,$$

which leads to:

$$c = \max_{x,y} |\alpha_{x,y}|^2, \quad (21)$$

where c depends only on the QW parameters, and remains unaffected by both channel noise and the protocol design. It represents the maximum probability of any outcome (x, y) , so lower c values yield a more uniform distribution (i.e., improved security), limiting an eavesdropper's ability to infer key information. By choosing F , t , ϕ , and θ appropriately, Alice and Bob can optimize both security and key rate. Importantly, this proof applies to any regular topology, not just the hypercube, as it is independent of the specific graph structure.

5 Qiskit models for quantum walks and QKD protocols

In this section, we first present the model underlying quantum walks and the subsequent QKD protocols constructed on two distinct topologies: circle and hypercube. Built upon the framework established by Douglas et al. [16], as also discussed in Section 2, this model structures the quantum walk using increment and decrement operations implemented with X (i.e., NOT) gates and multi-controlled X gates (i.e., MCX), which serve as the fundamental building blocks for both topologies.

5.1 Qiskit implementation of quantum walks

In this subsection, we present the implementation of circle and hypercube-based QWs, with evolution defined as detailed in Subsections 3.2 and 3.3. In circle-based walks, the walker’s position is encoded in $n = \lceil \log_2(2P) \rceil$ qubits, while a single coin qubit undergoes a unitary rotation parameterized by angles θ and ϕ (Equation 4). The walker is initialized in the computational basis (\mathcal{Z}), and conditional shifts are applied: if the coin is $|1\rangle$, the walker moves right; if $|0\rangle$, left. These shifts are implemented via multi-controlled X gates, and an additional operator $F \in \{I, X, Y\}$ is applied to the coin before each step to balance the distribution. The hypercube walk follows the same principles with a larger register: the walker’s position is encoded by P qubits, and P coin qubits determine movement along each dimension. Each step applies a coin operation (generic rotation or Grover coin) followed by dimension-dependent MCX shifts. The F operator and coin principles are applied as in the circle model, preserving modularity and extending naturally to higher dimensions. As detailed in Appendix B, we provide the Qiskit implementations of the circle and hypercube-based quantum walk topologies. In both cases, the QWs are initialized with X gates to set the states in the computational basis. An alternative is the Hadamard walk, where H gates create superpositions [50], but this is unsuitable for our scenario: applying H to $|0\rangle$ yields a superposition that remains unchanged after an X gate, preventing proper initialization on a computational basis. Regarding measurement, the reversal ensures that the walker’s readout matches the register, proceeding from the most significant bit (MSB) to the least significant bit (LSB). Finally, to approximate a randomized QW, larger values of t are required. Our simulations show that for $t \approx 10^3$ the distribution becomes nearly uniform across all walker states, but in the hypercube case this occurs only with a generic coin rotation rather than Grover’s coin.

5.2 Qiskit implementation of one-way QKD protocol

Building upon the quantum walk models and their implementation introduced in the previous subsection, we present the Qiskit-based implementation of our one-way QKD protocol on both circle and hypercube topologies. These realizations reuse the circuits and operators defined earlier, showing how the same QW

predictability. Since t affects noise tolerance, we aim to determine the value that maximizes noise resistance for a given walk configuration. Additionally, if this QKD protocol were implemented in practice, the definition of “optimal” would likely differ, requiring Alice and Bob to account for device imperfections and other practical constraints. It is important to emphasize that all of our simulations (both in this section and the following ones) are conducted using a Virtual Machine (VM) with the hardware specifications outlined in Table 1.

Table 1. Hardware specifications of the VM used for simulations.

Hardware	Specifications
CPU	Intel Core Processor (Haswell) pc-q35-2.11 CPU @ 2.0 GHz
Cores	12
RAM	31 GiB
Disk(s)	vda (32 G), vdb (300 G)
OS	Ubuntu 24.04 LTS
GPU	Red Hat, Inc. QXL paravirtual graphic card (rev 04)

We analyze different walk parameters to determine the minimum value c when $F = I$. To achieve this, we developed multiple scripts to simulate the QW using the Qiskit models defined in Section 5. We run the simulations for QW steps t ranging from 1 to 5×10^4 to identify the optimal t that minimizes c . For this evaluation, we used the generic coin rotation operator (consider Equation 4) with $\phi = 0$ and $\theta = \pi/4$. In the following subsections, we begin by reproducing and validating the state-of-the-art results presented by Vlachou et al. [51], using a Qiskit-based implementation that significantly differs from the original model adopted by the authors. Subsequently, we enhance the protocol’s security performance by introducing quantum walks on a hypercube topology.

6.1 Verification of state-of-the-art results

In this subsection, we first replicate the state-of-the-art results reported by Vlachou et al. [51], comparing their c and optimal t values with those obtained from our hypercube-based QWs to establish a reference for our analysis. The results of our initial evaluation are presented in Figure 2.

It is important to highlight that we replicate the results from Vlachou et al. [51] using a Qiskit-based model, which represents an entirely different approach compared to the simulations performed before this work. However, the results are consistent, given the differences in the two methods. As can be observed from Figure 2, we considered odd values of P ranging from 1 to 229 in order to align with the original analysis presented by Vlachou et al. [51], since only odd values of P are meaningful in the circle topology [1]. Using even values of P would restrict the support of the probability amplitudes to either even or odd numbered nodes, increasing the overall value of $|\alpha_{x,y}|$. In addition, for $P = 1$, we obtain $c = 0.5$, which matches the expected result for a classical BB84 protocol (i.e.,

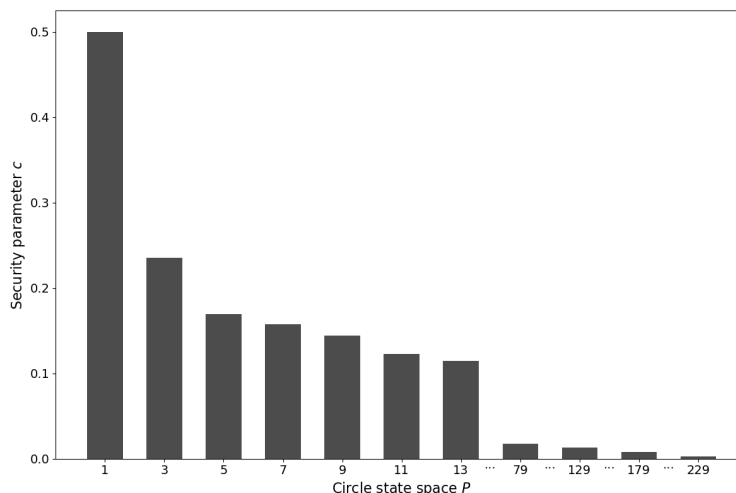


Fig. 2. Minimal security parameter c obtained for each position space dimension P in the circle topology, using $\phi = 0$, $\theta = \pi/4$, and $F = I$. It is important to note that a smaller value of c is more advantageous for Alice and Bob. Additionally, P represents the dimension of the position space. This serves as our state-of-the-art, from which we begin our analysis to improve performance.

when $P = 1$, our model collapses into the BB84). For all other values of P , as P increases, we observe smaller values of c with a reasonable t .

6.2 Hypercube-based quantum walks results

In this subsection, we analyze the security of our protocol when the underlying QWs are performed on the hypercube topology. In this configuration, the state space grows exponentially with P , reaching a dimension of 2^P , in contrast to the linear growth $2P$ in the circle. As a result, the probability amplitude naturally spreads across many possible outcomes, reducing the likelihood that any single outcome becomes dominant. This wider distribution is expected to lower the value of c , thereby enhancing the protocol's security by making the quantum states more difficult to predict. To allow a more precise comparison, we used the same parameters as in the circle-based simulations when evaluating the hypercube-based case. However, due to the limitations of the `AerSimulator` in the Qiskit environment [36], we are unable to simulate hypercube-based QWs for $P > 13$. Therefore, we will compare the results for $P \leq 13$, as shown in Figure 3. As specified earlier, our QKD protocol aims to produce a uniform distribution of states, reducing predictability for an eavesdropper. The Grover coin, however, introduces a bias tied to the public initialization state [32], making outcomes predictable with high probability. Referring to Equation 21, with $P = 1$ we expect $c = 0.5$, while larger P should lower c given sufficient iterations. Yet,

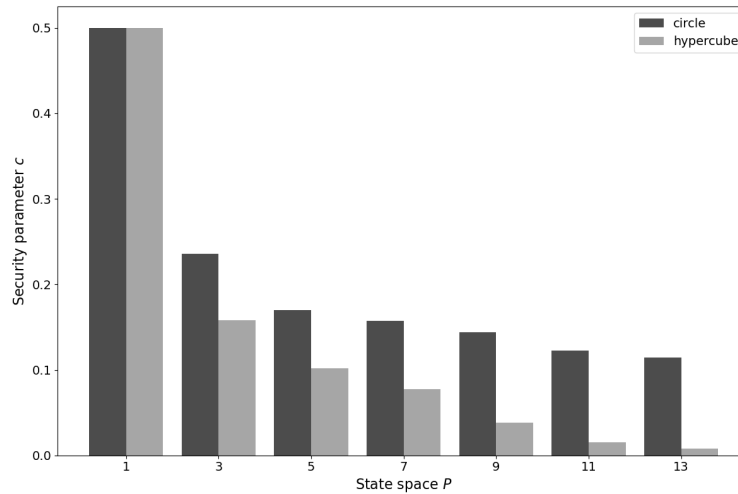


Fig. 3. Comparison plot between hypercube and circle-based quantum walks using the same parameters. The minimal value of c for each position space dimension P is shown for both topologies, with $\phi = 0$, $\theta = \pi/4$, and $F = I$. It’s important to note that Alice and Bob are better off with a smaller c , and P denotes the position space dimension.

with Grover coin on hypercubes, c remains fixed at 0.5 even as P grows, effectively collapsing the protocol to BB84. For this reason, we exclude Grover coin-based QWs from further study, noting this is an experimental conclusion rather than a formal proof. In contrast, hypercube-based walks with a generic rotation coin significantly outperform circle-based ones, yielding much lower c values with a reasonable number of steps (i.e., $t \approx 10^3$). This advantage comes from the exponentially larger and structured state space, which spreads probability more uniformly and limits distribution on specific outcomes. However, this comes at the cost of increased implementation complexity, as the hypercube-based QWs requires a higher number of qubits. Therefore, a trade-off must be considered between implementation feasibility and security, which is notably enhanced through the hypercube topology. To conclude, Table 2 compares the two topologies, highlighting their differences and improvements.

7 Noise resistance analysis

In this section, we analyze the robustness of our QKD protocol under noise. Using the parameters from the security analysis, we determine the optimal QW configuration for a given P and the corresponding c , then compute the secret key rate r and identify noise levels where $r > 0$. A physical implementation is not yet possible; otherwise, one could measure $p_{i,j}^z$ and $p_{i,j}^w$ (Equation 16) to calculate $H(A_z|B_z)$ and $H(A_w|B_w)$ for Equation 15. Since such an implementation does not yet exist, we have to consider noise models to estimate the QER of the QKD

Table 2. Comparison of the minimal values of c and optimal t for circle-based and hypercube-based quantum walks QKD protocol with $\phi = 0$, $\theta = \pi/4$, and $F = I$.

P	circle		hypercube	
	c	optimal t	c	optimal t
1	0.5	1	0.5	1
3	0.236	1084	0.158	1492
5	0.170	1196	0.102	1162
7	0.157	1202	0.077	965
9	0.144	1032	0.038	1085
11	0.123	1594	0.0154	1283
13	0.114	932	0.008	1378

protocol based on the type of QW employed, a standard approach referenced in several works [4,51].

7.1 Non-optimized protocol robustness

This subsection describes the noise models used to evaluate the maximum tolerable QER for a positive key rate (i.e., $r > 0$) and to assess protocol robustness. For replicability, we employ Qiskit’s built-in single-qubit noise models: depolarizing error [39] and combined amplitude-phase damping error [19,37,46,24], which simulate realistic quantum channel noise [25]. Depolarizing error models random perturbations from imperfect gates, while amplitude damping describes energy loss, such as photon loss or qubit relaxation [28,17], and phase damping captures dephasing, reducing coherence without changing populations [46,24,40]. Using a unified amplitude-phase damping model simplifies simulations, ensures consistency across qubits, and provides accurate QER estimates efficiently. Errors are applied via `add_all_qubit_quantum_error` [38], affecting both walker and coin qubits. While less precise than custom multi-qubit models [51], this approach prioritizes replicability and practical implementation. Furthermore, formal definitions of the noise models used are given in Appendix C. The maximally tolerated QER, measuring discrepancies between Alice and Bob when using the same basis, is defined as:

$$Q = \sum_{a \neq b} p_{a,b}^z = \mathbb{P}(A_z = a, B_z = b \mid w_A = w_B = 0), \quad (22)$$

which represents the probability that Alice and Bob obtain different outcomes when both measure in the \mathcal{Z} basis [51]. Since QER accounts for noise and potential eavesdropping, it is a key security metric in our QKD protocol. In fact, a high QER indicates excessive noise or an adversary’s interference. As a consequence, if it surpasses a critical threshold (i.e., 11 – 12% in BB84), error correction and privacy amplification become ineffective, making secure key extraction impossible. In our simulation, we use a depolarizing channel with a parameter λ set to match the maximum noise tolerance observed in the BB84 protocol (i.e., when $P = 1$ and $t = 1$), corresponding to a noise threshold $Q \approx 0.11 - 0.12$. For

higher P values, which correspond to a QW-based evolution, the same λ value is used to simulate the QKD protocol, ensuring consistent evaluation across different topologies and parameter settings. The same approach is applied to the amplitude-phase damping noise model simulations, where the amplitude and phase damping parameters were selected based on the same reasoning. Let's examine the results obtained for the hypercube-based and circle-based QKD protocols under depolarizing and amplitude-phase damping noise. The outcomes of the simulations under the two noise models are shown in Figure 4.

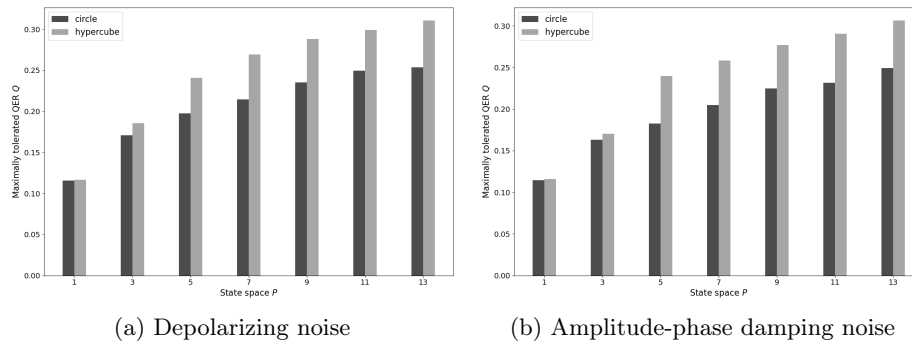


Fig. 4. Comparison of the maximally tolerated QER for circle and hypercube-based QKD protocols under depolarizing and amplitude-phase damping noise, using $F = I$, $\phi = 0$, and $\theta = \pi/4$. For $P = 1$, the BB84 limit is recovered, while at $P = 13$, the hypercube-based protocol achieves $Q \approx 0.311$ under depolarizing noise and $Q \approx 0.306$ under amplitude-phase damping, showing improved noise tolerance.

The results of Vlachou et al. [51] differ slightly, as they used a customized generalized Pauli noise model, better suited to their setup. For our simulations, the number of iterations was fixed at $N = 10^4$ to ensure reliable estimates of the QER, given the need for sufficient cases where $w_A = w_B = 0$. As shown in Figure 4, the hypercube-based QKD protocol shows higher noise tolerance than the circle-based one. In the circular case, each node connects to only two neighbors ($2P$ states), keeping the walk localized longer and making it more vulnerable to accumulated errors [22]. In contrast, the hypercube connects each node to P neighbors (2^P states), allowing exponential spreading that distributes noise more evenly and reduces its impact [30]. Under depolarizing noise, the circle's confinement leads to correlated errors [26], whereas the hypercube spreads states across a larger Hilbert space, mitigating noise per state. A similar effect occurs with amplitude-phase damping, where decoherence distributes over more dimensions [3]. Overall, the hypercube structure enhances resilience by enabling efficient error distribution, faster mixing, and reduced decoherence, thus supporting secure key generation at higher noise levels. Finally, detailed results are reported in Table 3.

Table 3. Comparison of the maximally tolerated QER results for circle-based and hypercube-based QKD protocols under the two noise types: depolarizing noise (Q_{dep}) and amplitude-phase damping noise (Q_{dmp}), with parameters fixed as $F = I$, $\phi = 0$, and $\theta = \pi/4$.

P	circle			hypercube		
	optimal t	Q_{dep}	Q_{dmp}	optimal t	Q_{dep}	Q_{dmp}
1	1	0.116	0.115	1	0.117	0.116
3	1084	0.171	0.163	1492	0.185	0.170
5	1196	0.198	0.183	1162	0.241	0.240
7	1202	0.215	0.205	965	0.269	0.258
9	1032	0.235	0.225	1085	0.288	0.277
11	1594	0.250	0.231	1283	0.299	0.290
13	932	0.253	0.249	1378	0.311	0.306

7.2 Parameters optimization

This subsection analyzes the selection of optimal parameters for our QKD protocol to maximize security (Section 6) and noise resistance (Section 7). We minimize c and maximize the tolerated QER (Q) by adjusting the operator F (from I to \tilde{X} or Y) to place the coin qubit(s) in superposition, and varying $\theta, \phi = \{k\pi/10 \mid k = 0, \dots, 10\}$ for the coin rotation. Optimal parameters are identified by first minimizing c for maximal security, then applying them in simulations of the circle or hypercube-based QKD protocol to evaluate the maximally tolerated QER under the noise models of Section 7. The optimal parameter combinations for both topologies are reported in Table 4.

Table 4. Optimal parameter settings F, ϕ, θ minimizing c and corresponding optimal number of steps t for both circle and hypercube configurations across different $P \neq 1$ values.

P	circle					hypercube				
	F	ϕ	θ	c	optimal t	F	ϕ	θ	c	optimal t
3	Y	0	0.3π	0.167	1322	Y	0	0.5π	0.109	1514
5	Y	0	0.5π	0.106	1466	\tilde{X}	0.2π	0.8π	0.080	1398
7	Y	0.5π	0.7π	0.083	1638	Y	0.5π	0.4π	0.045	1611
9	\tilde{X}	0.5π	0.8π	0.068	1296	Y	0.4π	0.6π	0.017	1235
11	Y	0.5π	0.3π	0.055	1374	Y	0.2π	0.8π	0.009	1750
13	Y	0.5π	0.9π	0.046	1503	Y	0.5π	0.3π	0.004	1198

From Table 4, optimal performance consistently requires $F \neq I$. Choosing $F = \tilde{X}$ or $F = Y$ produces nearly uniform output distributions, crucial for security, whereas $F = I$ generally degrades protocol performance. In Figure 5, we compare the maximum tolerated QER for circle-based and hypercube-based QKD protocols under depolarizing and amplitude-damping noise models, utilizing the optimal parameters listed in Table 4.

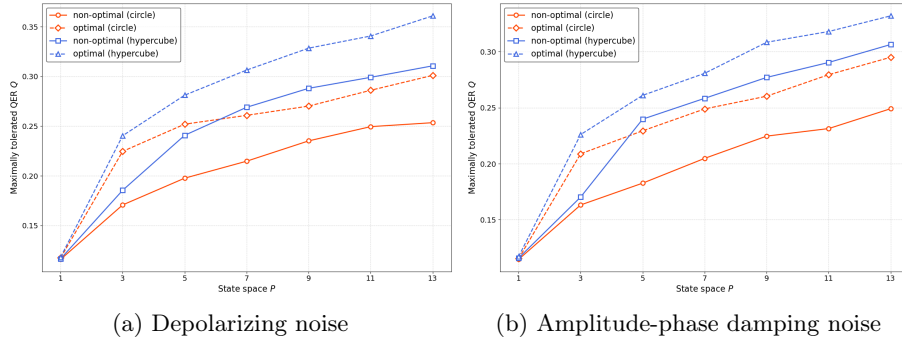


Fig. 5. Comparison of the maximum tolerated QER for circle-based and hypercube-based QKD under different noise types, using optimal parameters from Table 4. The hypercube-based protocol shows greater error tolerance: up to $Q \approx 0.361$ (depolarizing) and $Q \approx 0.332$ (amplitude-phase damping).

As shown in Figure 5, with an increase in P , both topologies exhibit an increase in QER, with the hypercube consistently tolerating higher QER values, reflecting its better noise resilience. This advantage is most evident at smaller P , where the system transitions from a BB84 protocol (i.e., $P = 1$) to a multi-qubit QKD protocol. The hypercube’s higher dimensionality offers better noise tolerance, keeping QER more stable at smaller P for secure QKD protocols. Moreover, parameter optimization improves performance, with optimal cases outperforming non-optimal ones. While the hypercube continues to perform better at larger P , the difference decreases as system complexity grows. These trends are consistent across various values of ϕ and θ , highlighting the importance of topology and optimization in QER, particularly during the transition to multi-qubit QKD protocols. In conclusion, Table 5 presents the optimal QER results for each P along with the corresponding parameters for our QKD protocol under both noise conditions.

Table 5. Optimal values for c , Q_{dep} , and Q_{dmp} in circle and hypercube configurations shown in Table 4, with Q_{dep} and Q_{dmp} representing the maximally tolerated QER for depolarizing and amplitude-phase damping noise, respectively.

P	circle			hypercube		
	c	Q_{dep}	Q_{dmp}	c	Q_{dep}	Q_{dmp}
3	0.167	0.225	0.209	0.109	0.240	0.226
5	0.106	0.252	0.229	0.080	0.281	0.261
7	0.083	0.261	0.249	0.045	0.306	0.281
9	0.068	0.270	0.260	0.017	0.329	0.308
11	0.055	0.286	0.280	0.009	0.341	0.318
13	0.046	0.301	0.295	0.004	0.361	0.332

8 Discussion and future work

In this section, we delve into the limitations of this research and propose directions for future work to build upon our results. We specifically focus on our proposed hypercube-based quantum walks QKD protocol, discussing its current constraints, potential vulnerabilities to practical attacks, and then exploring directions for further improvement and theoretical analysis.

Limitations and practical attacks. While our protocol proves more secure and noise-resistant than state-of-the-art schemes, several limitations still need to be addressed. First, due to `AerSimulator` constraints, we could only simulate up to $P \leq 13$. Larger values of P may further improve performance, though saturation in QER is possible. The hypercube protocol also requires more qubits, raising computational costs compared to the circle-based version. Moreover, our analysis relied on Qiskit’s single-qubit noise models for reproducibility, but a tailored multi-qubit model would yield a more realistic evaluation. Increasing iterations ($N \gg 10^4$) would improve QER estimates, though our hardware limited this. Similarly, the absence of a true RNG constrained the randomness of w_A, w_B , and $|i_A\rangle$, a limitation solvable with access to quantum RNGs. From a security perspective, the protocol does not depend on quantum memory. In the prepare-and-measure version, Eve requires a stable memory to attack, while Alice and Bob do not. The same holds for the entanglement-based scheme. Against practical threats such as photon-number-splitting [9], decoy states [21] remain effective, and our one-way communication model supports this countermeasure. However, authentication of the classical reconciliation channel is still essential to prevent man-in-the-middle attacks. Other known attacks, including Trojan Horse [49], detector blinding, and time-shift [29], can be mitigated with standard countermeasures [20,52,58]. Nonetheless, since our protocol involves more quantum states than traditional ones, its practical implementation may introduce new challenges that merit further study.

Future work. Several directions remain open for future work. Although our Qiskit model is functionally correct, more efficient implementations of QWs could be explored, as our choice of MCX gates and the coined model was guided mainly by feasibility. Alternative quantum walk models [50] might yield better performance. Similarly, while we avoided the Grover coin due to its unsuitability in one-way QKD, investigating other coin operators beyond a simple rotation could be worthwhile. Our security proof (Subsection 4.2) could also be strengthened, for example by deriving analytical expressions for optimal QW parameters or for c in Equation 21. Another open question is the asymptotic noise tolerance as the walk dimension grows (i.e., $P \rightarrow \infty$, possibly $t \rightarrow \infty$). Prior work on high-dimensional QKD (without walks) showed tolerance up to 50% disturbance [11], raising the question of whether our protocol approaches similar thresholds. Moreover, our analysis is limited to the sifting phase and does not extend to information reconciliation and privacy amplification steps. Information reconciliation can be carried out using classical methods such as Cascade [10],

LDPC codes [31], or BCH codes [48], consistent with our one-way communication model. Afterward, privacy amplification could be performed with universal hash functions [7] or Toeplitz-based constructions [23], which compress the reconciled raw key and remove any residual information accessible to Eve, resulting in a secure final key. Finally, concrete proposals for practical implementation also remain an important aspect for future work.

9 Conclusions

In this paper, we propose a novel one-way QKD protocol based on quantum walks over a hypercube topology. We also provide the first Qiskit implementation and simulation of one-way QKD using quantum walks on both circle and hypercube graphs, designing two versions: one exploiting the circle's symmetry and the other leveraging the hypercube's high connectivity. Our prepare-and-measure framework, built entirely in Qiskit, supports arbitrary topologies and built-in noise models (e.g., depolarizing, amplitude-phase damping), enabling a detailed performance comparison under realistic conditions. To ensure flexibility and reproducibility, all code and results are publicly available on GitHub. Our findings confirm recent results by Yu et al. [56] that high-dimensional systems are more noise-resilient than qubit-based schemes. In particular, quantum-walk states in a hypercube show superior noise robustness and security compared to the state-of-the-art, as detailed in Sections 6 and 7, despite the limitations discussed in Section 8. While practical implementation poses challenges (especially in realizing high-dimensional walks) recent advances in quantum walks and high-dimensional state engineering suggest feasibility in current photonic and simulator platforms. Crucially, robustness does not rely solely on large dimensions, indicating that experimental realization may already be feasible to implement. Overall, our results highlight quantum walks, especially on hypercubes, as a powerful and flexible approach to secure quantum communication.

References

1. Aharonov, D., Ambainis, A., Kempe, J., Vazirani, U.: Quantum walks on graphs. In: Proceedings of the Thirty-Third Annual ACM Symposium on Theory of Computing. p. 50–59. STOC '01, Association for Computing Machinery, New York, NY, USA (2001). <https://doi.org/10.1145/380752.380758>
2. Aharonov, Y., Davidovich, L., Zagury, N.: Quantum random walks. *Phys. Rev. A* **48**, 1687–1690 (Aug 1993). <https://doi.org/10.1103/PhysRevA.48.1687>
3. Allati, A.E., Baz, M.E.: Quantum key distribution using optical coherent states via amplitude damping. *Optical and Quantum Electronics* **47**(5), 1035–1046 (2015). <https://doi.org/10.1007/s11082-014-9959-2>
4. Bae, J., Acín, A.: Key distillation from quantum channels using two-way communication protocols. *Phys. Rev. A* **75**, 012334 (Jan 2007). <https://doi.org/10.1103/PhysRevA.75.012334>
5. Bennett, C.H., Brassard, G.: Quantum cryptography: Public key distribution and coin tossing. *Theoretical Computer Science* **560**, 7–11 (2014). <https://doi.org/10.1016/j.tcs.2014.06.026>

- 1016/j.tcs.2014.05.025, theoretical Aspects of Quantum Cryptography – celebrating 30 years of BB84
6. Bennett, C.H., Brassard, G., Mermin, N.D.: Quantum cryptography without bell’s theorem. *Phys. Rev. Lett.* **68**, 557–559 (Feb 1992). <https://doi.org/10.1103/PhysRevLett.68.557>
 7. Bennett, C.H., Brassard, G., Robert, J.M.: Privacy amplification by public discussion. *SIAM Journal on Computing* **17**(2), 210–229 (1988). <https://doi.org/10.1137/0217014>
 8. Berta, M., Christandl, M., Colbeck, R., Renes, J.M., Renner, R.: The uncertainty principle in the presence of quantum memory. *Nature Physics* **6**(9), 659–662 (Sep 2010). <https://doi.org/10.1038/nphys1734>
 9. Brassard, G., Lütkenhaus, N., Mor, T., Sanders, B.C.: Security aspects of practical quantum cryptography. In: Preneel, B. (ed.) *Advances in Cryptology – EUROCRYPT 2000*. pp. 289–299. Springer Berlin Heidelberg (2000). https://doi.org/10.1007/3-540-45539-6_20
 10. Brassard, G., Salvail, L.: Secret-key reconciliation by public discussion. In: Hellese, T. (ed.) *Advances in Cryptology - EUROCRYPT ’93*. pp. 410–423. Springer Berlin Heidelberg (1994). https://doi.org/10.1007/3-540-48285-7_35
 11. Chau, H.F.: Quantum key distribution using qudits that each encode one bit of raw key. *Phys. Rev. A* **92**, 062324 (Dec 2015). <https://doi.org/10.1103/PhysRevA.92.062324>
 12. Christandl, M., König, R., Renner, R.: Postselection technique for quantum channels with applications to quantum cryptography. *Phys. Rev. Lett.* **102**, 020504 (Jan 2009). <https://doi.org/10.1103/PhysRevLett.102.020504>
 13. Curty, M., Gühne, O., Lewenstein, M., Lütkenhaus, N.: Detecting two-party quantum correlations in quantum-key-distribution protocols. *Phys. Rev. A* **71**, 022306 (Feb 2005). <https://doi.org/10.1103/PhysRevA.71.022306>
 14. Curty, M., Lewenstein, M., Lütkenhaus, N.: Entanglement as a precondition for secure quantum key distribution. *Phys. Rev. Lett.* **92**, 217903 (May 2004). <https://doi.org/10.1103/PhysRevLett.92.217903>
 15. Devetak, I., Winter, A.: Distillation of secret key and entanglement from quantum states. *Proceedings: Mathematical, Physical and Engineering Sciences* **461**(2053), 207–235 (2005), <http://www.jstor.org/stable/30046924>
 16. Douglas, B.L., Wang, J.B.: Efficient quantum circuit implementation of quantum walks. *Phys. Rev. A* **79**, 052335 (May 2009). <https://doi.org/10.1103/PhysRevA.79.052335>
 17. Dutta, S., Biswas, D., Mandayam, P.: Noise-adapted qudit codes for amplitude-damping noise. *Phys. Rev. A* **111**, 032438 (Mar 2025). <https://doi.org/10.1103/PhysRevA.111.032438>
 18. Ekert, A.K.: Quantum cryptography based on bell’s theorem. *Phys. Rev. Lett.* **67**, 661–663 (Aug 1991). <https://doi.org/10.1103/PhysRevLett.67.661>
 19. Fortes, R., Rigolin, G.: Fighting noise with noise in realistic quantum teleportation. *Phys. Rev. A* **92**, 012338 (Jul 2015). <https://doi.org/10.1103/PhysRevA.92.012338>
 20. Gisin, N., Fasel, S., Kraus, B., Zbinden, H., Ribordy, G.: Trojan-horse attacks on quantum-key-distribution systems. *Physical Review A* **73**(2) (Feb 2006). <https://doi.org/10.1103/physreva.73.022320>
 21. Hwang, W.Y.: Quantum key distribution with high loss: Toward global secure communication. *Phys. Rev. Lett.* **91**, 057901 (Aug 2003). <https://doi.org/10.1103/PhysRevLett.91.057901>

22. Keating, J.P., Linden, N., Matthews, J.C.F., Winter, A.: Localization and its consequences for quantum walk algorithms and quantum communication. *Phys. Rev. A* **76**, 012315 (Jul 2007). <https://doi.org/10.1103/PhysRevA.76.012315>
23. Krawczyk, H.: Lfsr-based hashing and authentication. In: Desmedt, Y.G. (ed.) *Advances in Cryptology – CRYPTO '94*. pp. 129–139. Springer Berlin Heidelberg (1994). https://doi.org/10.1007/3-540-48658-5_15
24. Kristensen, L.B., Kjaergaard, M., Andersen, C.K., Zinner, N.T.: Hybrid quantum error correction in qubit architectures. *Phys. Rev. A* **108**, 022403 (Aug 2023). <https://doi.org/10.1103/PhysRevA.108.022403>
25. Lasota, M., Kovalenko, O., Usenko, V.C.: Robustness of entanglement-based discrete and continuous-variable quantum key distribution against channel noise. *New Journal of Physics* **25**(12), 123003 (Dec 2023). <https://doi.org/10.1088/1367-2630/ad0e8c>
26. Li, J.X., Lu, F.Y., Wang, Z.H., Zapatero, V., Curty, M., Wang, S., Yin, Z.Q., Chen, W., He, D.Y., Guo, G.C., Han, Z.F.: Quantum key distribution overcoming practical correlated intensity fluctuations. *npj Quantum Information* **11**(1), 106 (2025). <https://doi.org/10.1038/s41534-025-01059-0>
27. Lo, H.K., Chau, H.F.: Unconditional security of quantum key distribution over arbitrarily long distances. *Science* **283**(5410), 2050–2056 (1999). <https://doi.org/10.1126/science.283.5410.2050>
28. Lonigro, D., Chruściński, D.: Excitation-damping quantum channels. *Journal of Physics A: Mathematical and Theoretical* **56**(25), 255301 (May 2023). <https://doi.org/10.1088/1751-8121/acd734>
29. Lydersen, L., Wiechers, C., Wittmann, C., Elser, D., Skaar, J., Makarov, V.: Hacking commercial quantum cryptography systems by tailored bright illumination. *Nature Photonics* **4**(10), 686–689 (Aug 2010). <https://doi.org/10.1038/nphoton.2010.214>
30. Majury, H., Boutari, J., O’Sullivan, E., Ferraro, A., Paternostro, M.: Robust quantum state engineering through coherent localization in biased-coin quantum walks. *EPJ Quantum Technology* **5**(1), 1 (2018). <https://doi.org/10.1140/epjqt/s40507-017-0065-9>
31. Mesiti, F., Delgado, M., Mondin, M., Daneshgaran, F.: Sparse-graph codes for information reconciliation in qkd applications. In: *2010 3rd International Symposium on Applied Sciences in Biomedical and Communication Technologies (ISABEL 2010)*. pp. 1–5 (2010). <https://doi.org/10.1109/ISABEL.2010.5702882>
32. Nahimovs, N., Rivosh, A.: Exceptional configurations of quantum walks with grover’s coin. In: Kofroň, J., Vojnar, T. (eds.) *Mathematical and Engineering Methods in Computer Science*. pp. 79–92. Springer International Publishing, Cham (2016). https://doi.org/10.1007/978-3-319-29817-7_8
33. Nielsen, M.A., Chuang, I.L.: *Quantum Computation and Quantum Information: 10th Anniversary Edition*. Cambridge University Press, Cambridge (2010). <https://doi.org/10.1017/CBO9780511976667>
34. Portugal, R.: *Quantum Walks and Search Algorithms*. Quantum Science and Technology, Springer Cham, 2 edn. (2018). <https://doi.org/10.1007/978-3-319-97813-0>
35. Qiang, X., Ma, S., Song, H.: Quantum walk computing: Theory, implementation, and application. *Intelligent Computing* **3**, 0097 (2024). <https://doi.org/10.34133/icomputing.0097>
36. Qiskit Development Team: *AerSimulator: Qiskit aer 0.17.1* (2025), https://qiskit.github.io/qiskit-aer/stubs/qiskit_aer.AerSimulator.html, accessed: 2025-09-08

37. Qiskit Development Team: Amplitude damping error: Qiskit aer 0.17.1 (2025), https://qiskit.github.io/qiskit-aer/stubs/qiskit_aer.noise.amplitude_damping_error.html, accessed: 2025-09-08
38. Qiskit Development Team: Building noise models: Qiskit aer 0.17.1 (2025), https://qiskit.github.io/qiskit-aer/tutorials/3_building_noise_models.html, accessed: 2025-09-08
39. Qiskit Development Team: Depolarizing error: Qiskit aer 0.17.1 (2025), https://qiskit.github.io/qiskit-aer/stubs/qiskit_aer.noise.depolarizing_error.html, accessed: 2025-09-08
40. Qiskit Development Team: Phase damping error: Qiskit aer 0.17.1 (2025), https://qiskit.github.io/qiskit-aer/stubs/qiskit_aer.noise.phase_damping_error.html, accessed: 2025-09-08
41. Qiskit Development Team: Qiskit inverse: IBM quantum documentation (2025), <https://docs.quantum.ibm.com/api/qiskit/qiskit.circuit.Instruction#inverse>, accessed: 2025-09-08
42. Renner, R.: Symmetry of large physical systems implies independence of subsystems. *Nature Physics* **3**(9), 645–649 (Sep 2007). <https://doi.org/10.1038/nphys684>
43. Renner, R., Gisin, N., Kraus, B.: Information-theoretic security proof for quantum-key-distribution protocols. *Physical Review A* **72**(1) (Jul 2005). <https://doi.org/10.1103/physreva.72.012332>
44. Rohde, P.P., Fitzsimons, J.F., Gilchrist, A.: Quantum walks with encrypted data. *Phys. Rev. Lett.* **109**, 150501 (Oct 2012). <https://doi.org/10.1103/PhysRevLett.109.150501>
45. Scarani, V., Bechmann-Pasquinucci, H., Cerf, N.J., Dušek, M., Lütkenhaus, N., Peev, M.: The security of practical quantum key distribution. *Rev. Mod. Phys.* **81**, 1301–1350 (Sep 2009). <https://doi.org/10.1103/RevModPhys.81.1301>
46. Shu, H., Zhang, C.Y., Chen, Y.Q., Zheng, Z.J., Fei, S.M.: Quantum key distribution over noisy channels by the testing state method. *International Journal of Theoretical Physics* **62**(8) (Jul 2023). <https://doi.org/10.1007/s10773-023-05393-x>
47. Tomamichel, M., Lim, C.C.W., Gisin, N., Renner, R.: Tight finite-key analysis for quantum cryptography. *Nature Communications* **3**(1), 634 (2012). <https://doi.org/10.1038/ncomms1631>
48. Traisilanun, W., Sripimanwat, K., Sangaroon, O.: Secret key reconciliation using bch code in quantum key distribution. In: 2007 International Symposium on Communications and Information Technologies. pp. 1482–1485 (2007). <https://doi.org/10.1109/ISCIT.2007.4392249>
49. Vakhitov, A., Makarov, V., Hjelle, D.R.: Large pulse attack as a method of conventional optical eavesdropping in quantum cryptography. *Journal of Modern Optics* **48**(13), 2023–2038 (2001). <https://doi.org/10.1080/09500340108240904>
50. Venegas Andraca, S.E.: Quantum walks: a comprehensive review. *Quantum Information Processing* **11**(5), 1015–1106 (Jul 2012). <https://doi.org/10.1007/s11128-012-0432-5>
51. Vlachou, C., Krawec, W., Mateus, P., Paunković, N., Souto, A.: Quantum key distribution with quantum walks. *Quantum Information Processing* **17**(11), 288 (2018). <https://doi.org/10.1007/s11128-018-2055-y>
52. Wang, J., Wang, H., Qin, X., Wei, Z., Zhang, Z.: The countermeasures against the blinding attack in quantum key distribution. *The European Physical Journal D* **70**(1), 5 (2016). <https://doi.org/10.1140/epjd/e2015-60469-8>
53. Woodhead, E., Pironio, S.: Secrecy in prepare-and-measure clausen-horne-shimony-holt tests with a qubit bound. *Phys. Rev. Lett.* **115**, 150501 (Oct 2015). <https://doi.org/10.1103/PhysRevLett.115.150501>

54. Xia, F., Liu, J., Nie, H., Fu, Y., Wan, L., Kong, X.: Random walks: A review of algorithms and applications. *IEEE Transactions on Emerging Topics in Computational Intelligence* **4**(2), 95–107 (Apr 2020). <https://doi.org/10.1109/tetci.2019.2952908>
55. Yao, A.C.C.: How to generate and exchange secrets. In: 27th Annual Symposium on Foundations of Computer Science (sfcs 1986). pp. 162–167 (1986). <https://doi.org/10.1109/SFCS.1986.25>
56. Yu, H., Sciara, S., Chemnitz, M., Montaut, N., Crockett, B., Fischer, B., Helsten, R., Wetzel, B., Goebel, T.A., Krämer, R.G., Little, B.E., Chu, S.T., Nolte, S., Wang, Z., Azaña, J., Munro, W.J., Moss, D.J., Morandotti, R.: Quantum key distribution implemented with d-level time-bin entangled photons. *Nature Communications* **16**(1), 171 (2025). <https://doi.org/10.1038/s41467-024-55345-0>
57. Zhang, P., Sagar, J., Hastings, E., Stefko, M., Joshi, S., Rarity, J.: End-to-end demonstration for cubesatellite quantum key distribution. *IET Quantum Communication* **5**(3), 291–302 (2024). <https://doi.org/10.1049/qt2.12093>
58. Zhao, Y., Fung, C.H.F., Qi, B., Chen, C., Lo, H.K.: Quantum hacking: Experimental demonstration of time-shift attack against practical quantum-key-distribution systems. *Phys. Rev. A* **78**, 042333 (Oct 2008). <https://doi.org/10.1103/PhysRevA.78.042333>

Appendix

This appendix collects additional material complementing the main paper. It first presents schematic representations of the proposed one-way and entanglement-based QKD schemes, illustrating their operational steps. It then introduces the Qiskit implementation schemes of the quantum walks used in our protocols. Finally, it provides the formal definitions of the quantum noise models adopted in our simulations, particularly depolarizing and amplitude-phase damping channels.

A One-way QKD and entanglement-based schemes

In this section, we present the proposed one-way QKD protocol based on quantum walks over a hypercube topology and its entanglement-based variant to illustrate its security. Figure 6 shows the main steps: Alice randomly selects a basis w_A and state index i_A , prepares the corresponding quantum state $|\psi_i\rangle$, and sends it to Bob. Bob randomly chooses a measurement basis w_B and measures the received state. Using a classical authenticated channel, they compare basis choices, keeping outcomes only when $w_A = w_B$ to form the raw key.

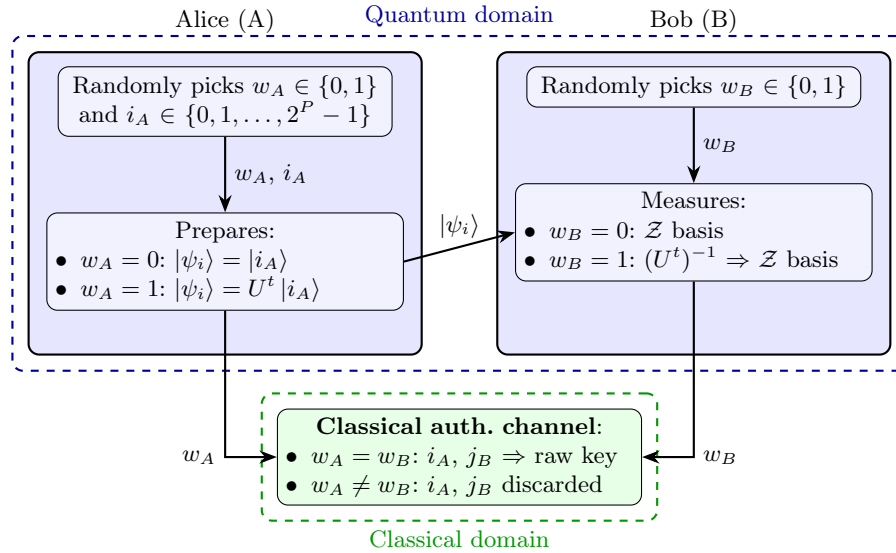


Fig. 6. Schematic representation of the proposed one-way hypercube-based QKD protocol. The arrow from Alice to Bob represents the transmission over the public quantum channel of the state $|\psi_i\rangle$ prepared by Alice, based on w_A and i_A . After the quantum communication, a classical authenticated channel is used to compare the basis choices (i.e., w_A, w_B) and extract the shared key.

To demonstrate the protocol’s security, Figure 7 depicts the entanglement-based version. Alice prepares a maximally entangled state $|\Psi_0\rangle$, keeps one half, and sends the other to Bob. Both parties randomly measure in the \mathcal{Z} or \mathcal{QW} basis, discarding outcomes when bases differ.

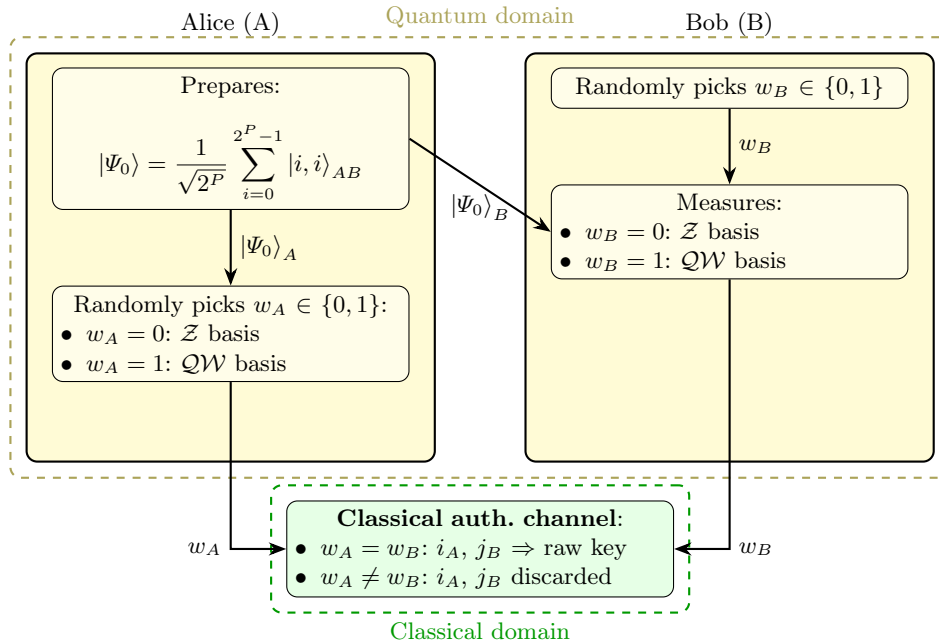


Fig. 7. Schematic representation of the entanglement-based one-way QKD protocol on a hypercube topology (see Figure 6). Alice prepares the entangled state $|\Psi_0\rangle$, retains one half, and sends the second half to Bob. Both parties perform measurements in a randomly selected basis (\mathcal{Z} or \mathcal{QW}), discarding outcomes when their basis choices differ.

Together, these representations provide a complete view of the hypercube-based QKD protocol, showing both practical prepare-and-measure operations and the entanglement-based scheme that underpins its security.

B Qiskit implementation of quantum walks

In this section, we present the Qiskit implementation of our quantum walk schemes, which serve as realistic circuit-level representations of the models described in the main work. Although achieving a nearly uniform distribution of states requires a large number of steps (i.e., $t \gg 1$), we restrict our discussion to the single-step case ($t = 1$) for clarity, since visualizing longer evolutions quickly becomes impractical. The presented circuits highlight how the position and coin

spaces are encoded in qubit registers, and how the walk operators is built from elementary quantum gates. Specifically, Figures 8 and 9 show the structures corresponding to the circle-based walk, and the hypercube walk with a generic rotation coin, respectively.

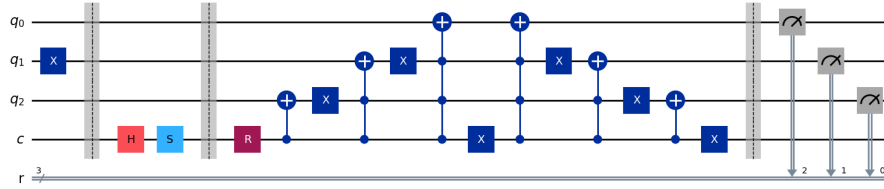


Fig. 8. Qiskit complete implementation of a circle-based quantum walk: $P = 3$, $t = 1$, $|\psi_0\rangle = |2\rangle = |(10)_2\rangle$, $F = Y$, $\phi = 0$, $\theta = \pi/4$.

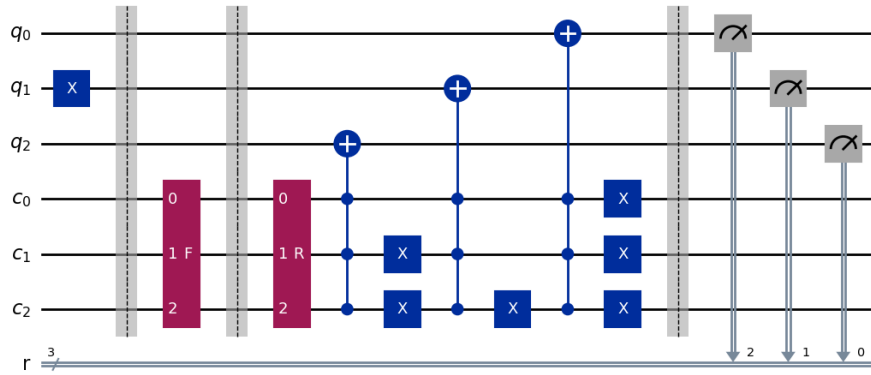


Fig. 9. Qiskit complete implementation of a hypercube-based quantum walk (generic coin): $P = 3$, $t = 1$, $|\psi_0\rangle = |2\rangle = |(10)_2\rangle$, $F = Y$, $\phi = 0$, $\theta = \pi/4$.

These implementations not only provide an illustrative reference for the theoretical framework but also demonstrate their feasibility on near-term quantum devices.

C Noise models: depolarizing and damping

In this section, we formally introduce the quantum noise models considered in our analysis. The depolarizing error model is formally defined as:

$$\mathcal{E}(\hat{\rho}) = (1 - \lambda)\hat{\rho} + \lambda \text{Tr}[\hat{\rho}] \frac{I}{2^n}, \quad (23)$$

where $\hat{\rho}$ denotes the density matrix of an n -qubit quantum state, λ is the depolarizing strength ($0 \leq \lambda \leq 4^n/4^n - 1$), and I is the $2^n \times 2^n$ identity operator. For $\lambda = 0$, the channel acts trivially, i.e., $\mathcal{E}(\hat{\rho}) = \hat{\rho}$, whereas for $\lambda = 1$, the state is fully randomized into the maximally mixed state $\mathcal{E}(\hat{\rho}) = I/2^n$, corresponding to complete information loss. When extending the analysis to amplitude-phase damping noise, we first consider the amplitude damping channel, defined by the following Kraus operators:

$$\begin{aligned} \hat{A}_0 &= \sqrt{1-p_a} \begin{bmatrix} 1 & 0 \\ 0 & \sqrt{1-a} \end{bmatrix}, \quad \hat{A}_1 = \sqrt{1-p_a} \begin{bmatrix} 0 & \sqrt{a} \\ 0 & 0 \end{bmatrix}, \\ \hat{A}_2 &= \sqrt{p_a} \begin{bmatrix} \sqrt{1-a} & 0 \\ 0 & 1 \end{bmatrix}, \quad \hat{A}_3 = \sqrt{p_a} \begin{bmatrix} 0 & 0 \\ \sqrt{a} & 0 \end{bmatrix}, \end{aligned} \quad (24)$$

where a quantifies the probability of energy decay ($|1\rangle \rightarrow |0\rangle$) and p_a encodes the initial population of the excited state. Moreover, the phase damping noise can be expressed through the following Kraus operators:

$$\hat{P}_0 = \begin{bmatrix} 1 & 0 \\ 0 & \sqrt{1-b} \end{bmatrix}, \quad \hat{P}_1 = \begin{bmatrix} 0 & 0 \\ 0 & \sqrt{b} \end{bmatrix}, \quad (25)$$

where b is the phase damping probability, with $b = 0$ yielding perfect coherence and $b = 1$ corresponding to full decoherence. Finally, the combined amplitude-phase damping channel is constructed via the product $\hat{K}_{ij} = \hat{P}_j \cdot \hat{A}_i$, producing the Kraus operators:

$$\begin{aligned} \hat{K}_{00} &= \hat{P}_0 \cdot \hat{A}_0 = \sqrt{1-p_a} \begin{bmatrix} 1 & 0 \\ 0 & \sqrt{(1-a)(1-b)} \end{bmatrix}, \\ \hat{K}_{01} &= \hat{P}_1 \cdot \hat{A}_0 = \sqrt{1-p_a} \begin{bmatrix} 0 & 0 \\ 0 & \sqrt{b(1-a)} \end{bmatrix}, \\ \hat{K}_{10} &= \hat{P}_0 \cdot \hat{A}_1 = \sqrt{1-p_a} \begin{bmatrix} 0 & \sqrt{a} \\ 0 & 0 \end{bmatrix}, \\ \hat{K}_{11} &= \hat{P}_1 \cdot \hat{A}_1 = \mathbf{0}, \\ \hat{K}_{20} &= \hat{P}_0 \cdot \hat{A}_2 = \sqrt{p_a} \begin{bmatrix} \sqrt{1-a} & 0 \\ 0 & \sqrt{1-b} \end{bmatrix}, \\ \hat{K}_{21} &= \hat{P}_1 \cdot \hat{A}_2 = \sqrt{p_a} \begin{bmatrix} 0 & 0 \\ 0 & \sqrt{b} \end{bmatrix}, \\ \hat{K}_{30} &= \hat{P}_0 \cdot \hat{A}_3 = \sqrt{p_a} \begin{bmatrix} 0 & 0 \\ \sqrt{a(1-b)} & 0 \end{bmatrix}, \\ \hat{K}_{31} &= \hat{P}_1 \cdot \hat{A}_3 = \sqrt{p_a} \begin{bmatrix} 0 & 0 \\ \sqrt{ab} & 0 \end{bmatrix}. \end{aligned} \quad (26)$$

Although $\hat{K}_{11} = \mathbf{0}$, this does not compromise the overall effect of the noise channel. Moreover, the presence of zero operators among the Kraus set does not affect the validity of the quantum operation, as they contribute nothing to the operator-sum $\sum_i \hat{K}_i^\dagger \hat{K}_i = I$. In this case, $\hat{K}_{11} = \hat{P}_1 \cdot \hat{A}_1 = \mathbf{0}$ simply reflects that the sequence of applying \hat{A}_1 (which maps $|1\rangle$ to $|0\rangle$) followed by \hat{P}_1 (which acts only on $|1\rangle$) yields no contribution, as their supports do not overlap. The set of Kraus operators $\{\hat{K}_{ij}\}$ (see Equation 26) provides a complete representation of the combined amplitude-phase damping effects within a single quantum channel, as shown below:

$$\mathcal{E}(\hat{\rho}) = \sum_{i=0}^3 \sum_{j=0}^1 \hat{K}_{ij} \hat{\rho} \hat{K}_{ij}^\dagger. \quad (27)$$

This formulation provides a complete and rigorous description of the depolarizing and amplitude-phase damping noise models used in our simulations.